

Principal Component Density Estimation for Scenario Generation Using Normalizing Flows

Eike Cramer^{a,b}, Alexander Mitsos^{c,a,d}, Raúl Tempone^{e,f}, Manuel Dahmen^{a,*}

^a Forschungszentrum Jülich GmbH, Institute of Energy and Climate Research, Energy Systems Engineering (IEK-10), Jülich 52425, Germany

^b RWTH Aachen University Aachen 52062, Germany

^c JARA-ENERGY, Jülich 52425, Germany

^d RWTH Aachen University, Process Systems Engineering (AVT.SVT), Aachen 52074, Germany

^e RWTH Aachen University, Institute of Uncertainty Quantification, Aachen 52062, Germany

^f King Abdullah University of Science and Technology, Department of Applied Mathematics and Computational Science, Jeddah, Saudi Arabia

Abstract: Neural networks-based learning of the distribution of non-dispatchable renewable electricity generation from sources such as photovoltaics (PV) and wind as well as load demands has recently gained attention. Normalizing flow density models have performed particularly well in this task due to the training through direct log-likelihood maximization. However, research from the field of image generation has shown that standard normalizing flows can only learn smeared-out versions of manifold distributions and can result in the generation of noisy data. To avoid the generation of time series data with unrealistic noise, we propose a dimensionality-reducing flow layer based on the linear principal component analysis (PCA) that sets up the normalizing flow in a lower-dimensional space. We train the resulting principal component flow (PCF) on data of PV and wind power generation as well as load demand in Germany in the years 2013 to 2015. The results of this investigation show that the PCF preserves critical features of the original distributions, such as the probability density and frequency behavior of the time series. The application of the PCF is, however, not limited to renewable power generation but rather extends to any data set, time series, or otherwise, which can be efficiently reduced using PCA.

Keywords:

renewable energy; scenario generation; normalizing flows; dimensionality reduction; principal component analysis

1 Introduction

The renewable electricity generation technologies photovoltaics (PV) and wind depend on natural occurrences and are therefore non-dispatchable. Additionally, the realization of these renewable power generation outputs exhibits uncertain and volatile behavior, which poses new challenges for the design and operation of energy systems compared to dispatchable fossil power generation (Agora Energiewende and Sandbag, 2020; Mitsos et al., 2018). To account for the uncertainty in renewable electricity sources and other relevant energy system parameters like electricity demands, scenarios are often utilized to represent possible realizations. Here, the term scenario refers to a possible realization of the uncertain and volatile parameter over a certain time span. A set of scenarios thus refers to a collection of time series of equal length. Scenarios can be applied in stochastic programming formulations for the design and operation of energy systems as well as energy-related scheduling tasks (Kaut and Wallace, 2003; Birge and Louveaux, 2011). The distributions of time series intervals are often unknown and consist of many non-independent dimensions due to the correlation between time steps. These distributions typically do not follow standard distribution models like multivariate Gaussians. Thus, sampling these distributions for scenario generation remains an open research question.

There are many contributions to the literature on how to generate scenarios. Contributions include the traditional Box-Jenkins approach (Box et al., 1967) for sampling stochastic processes (Sharma et al., 2013) as well as Gaussian mixture models (Wang et al., 2018), Copula methods (Kaut and Wallace, 2011), and moment matching techniques (Chopra and Selvamuthu, 2020). With the increase of computational

*Manuel Dahmen, Forschungszentrum Jülich GmbH, Institute of Energy and Climate Research, Energy Systems Engineering (IEK-10), Jülich 52425, Germany
E-mail: m.dahmen@fz-juelich.de

power and the development of advanced machine learning algorithms, it is now possible to train specialized artificial neural networks (ANNs) to learn distributions without any statistical assumptions about the data. These so-called deep generative models (DGMs) are trained on sets of scenarios created from historical time series. The equidistant segments of univariate scenarios are viewed as multidimensional points, e.g., a scenario of one day with hourly recordings is viewed as a 24-dimensional data point.

In 2018, Chen et al. (2018c) proposed the use of generative adversarial networks (GANs) (Goodfellow et al., 2014) for scenario generation. Since then, scenario generation using GANs and other DGMs has become a popular topic (Chen et al., 2018c; Jiang et al., 2018, 2019; Zhang et al., 2020; Wei et al., 2019; Zhang and Zhang, 2020). Chen et al. (2018c) later extended their original work by introducing a scenario selection procedure (Chen et al., 2018b) and by using Bayesian GANs (Chen et al., 2018a). Other examples of GANs for wind and PV power output scenarios are presented in (Jiang et al., 2018, 2019; Zhang et al., 2020). For more consistent convergence in training, the authors in Chen et al. (2018c); Jiang et al. (2018, 2019); Zhang et al. (2020) used Wasserstein GANs (Arjovsky et al., 2017) where they enforce a Lipschitz constraint on the critic network. Besides the generation of wind and PV scenarios, GAN-based scenario generation was also applied to residential load forecasts (Gu et al., 2019) and hydro-wind-solar hybrid systems (Wei et al., 2019). Schreiber et al. (2019) study different loss functions for GANs and found the Wasserstein distance to be superior to the binary-cross-entropy. Besides GANs, a popular type of DGMs are variational autoencoders (VAEs) (Kingma and Welling, 2014). Examples of VAEs for scenario generation include electric vehicle load demand (Pan et al., 2019), hydro wind-solar hybrid systems (Zhang et al., 2018), as well as hydro concentrated solar power hybrid systems (Qi et al., 2020).

Despite their recent success in scenario generation for renewable power generation, both GANs and VAEs show inconsistencies in training. Specifically, the Nash Equilibria obtained through GAN training are reported to be unstable, and there is no guarantee for the generator to sample from the target distribution (Arjovsky et al., 2017). The VAE uses the Evidence Lower Bound (ELBO) loss function in training which gives no concrete measure on the actual quality of the fit (Kingma and Welling, 2014).

In contrast to GANs and VAEs, a third DGM structure, normalizing flows (Dinh et al., 2017; Papamakarios et al., 2019), can directly fit the probability density function (PDF) of the unknown distribution by log-likelihood maximization. In theory, using a sufficiently expressive normalizing flow network and enough training data, the trained distribution will converge to the true distribution. However, normalizing flows are not as well established as GANs and VAEs in scenario generation, yet. To our knowledge, there are only two contributions that use normalizing flows in the context of energy systems by Zhang and Zhang (2020) and Ge et al. (2020) who both focus on residential load forecasts. Zhang and Zhang (2020) and Ge et al. (2020) employed standard normalizing flow structures, i.e., real non volume preserving transformation (realNVP) (Dinh et al., 2017) and nonlinear independent component estimation (NICE) (Dinh et al., 2015), respectively.

Recently, Gemici et al. (2016) and Brehmer and Cranmer (2020) showed that normalizing flows are by design unable to fit manifold distributions. Brehmer and Cranmer (2020) find that fitting a full dimensional normalizing flow to a manifold distribution results in a smeared-out version of the true distribution. Sampling from the smeared-out fit then leads to the samples outside of the true distribution. Gemici et al. (2016) suggest using normalizing flows on manifolds instead, i.e., to perform density estimation in a lower-dimensional space, but do not further elaborate on such an approach and do not report on any numerical experiments. Brehmer and Cranmer (2020) build normalizing flows in lower-dimensional space by fixing some of the latent space dimensions to a constant. We find that manifolds are frequently present in PV and wind power generation time series due to the temporal correlation between time steps. Thus, we argue that normalizing flows should be set up for density estimation with a lower-dimensional latent space to avoid the generation of unrealistic and out-of-distribution data.

As part of this paper, we provide the following contributions: We introduce an additional perspective on the effects of data manifolds on normalizing flow-based density estimation by eliciting the contradiction between manifolds and diffeomorphic transformations. Further, we argue how data manifolds can lead to the generation of unrealistic and out-of-distribution data. In addition, we present a novel modification of normalizing flows using a dimensionality reducing flow layer based on the principal component analysis (PCA) and show theoretically that the resulting principal component flow (PCF) does not affect the

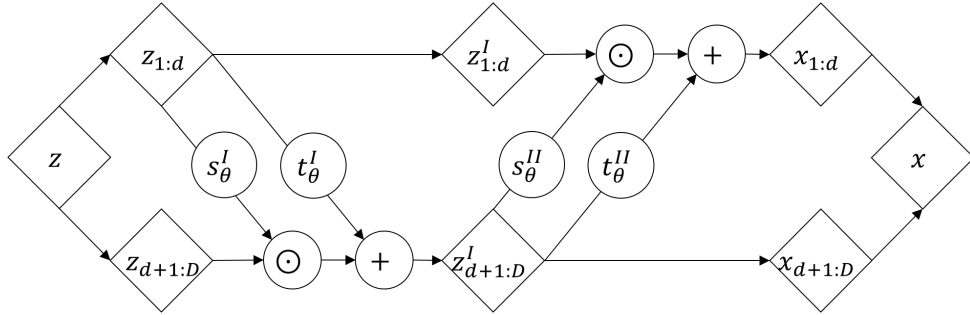


Fig. 1. Real non-volume preserving transformation (realNVP) (Dinh et al., 2017) with two coupling layers with alternating identity and affine transformations. Arrows point in generative direction. Compositions may include more than two coupling layers. Functions $s_\theta^I(z_{1:d})$, $t_\theta^I(z_{1:d})$, $s_\theta^{II}(z_{d+1:D})$, and $t_\theta^{II}(z_{d+1:D})$ are trainable ANNs with parameters θ .

density estimation procedure. In numerical experiments, we train the new PCF method on data of PV and wind power generation as well as load demand in Germany in the years 2013 to 2015. The results show that the PCF learns the data distribution better than the full space normalizing flow (FSNF) and also reproduces the frequency behavior of the original time series.

The remainder of this paper is organized as follows: In Section 2, we introduce the general concept of normalizing flows and review the realNVP affine coupling layer (Dinh et al., 2017) which will serve as the underlying flow structure in this paper. In Section 3, we continue the discussion started by Gemici et al. (2016) and Brehmer and Cranmer (2020) about the effects of manifolds on normalizing flows and present the novel PCF layer for density estimation in lower-dimensional latent space. In Section 4, we present the results of simulation studies on data of PV and wind power generation as well as load demand in Germany (Open power systems data, 2019). Finally, in Section 5 we conclude our work.

2 Density Estimation using Normalizing Flows

Normalizing flows are invertible transformations \mathbf{f} between a complex target distribution and a well-described base distribution, e.g., a multivariate Gaussian. Normalizing flows aim to model a complex distribution as a transformation of a simple one instead of manually deriving a complex model that fits the data. Thus, the sampling takes place in the known base distribution, and the transformation does not have to consider the randomness in the data.

A normalizing flow transformation must be set up as a diffeomorphism, i.e., both the forward and the inverse transformation must be continuously differentiable (Papamakarios et al., 2019). In their standard form, normalizing flows require equal dimensionality of base and target distributions, in which case the density of the target distribution is well described using the change of variables formula (CVF) (Papamakarios et al., 2019)

$$p_X(\mathbf{x}) = p_Z(\mathbf{f}^{-1}(\mathbf{x})) \cdot |\det(\mathbf{J}_{\mathbf{f}^{-1}}(\mathbf{x}))|, \quad (1)$$

where $p_X(\mathbf{x})$ and $p_Z(\mathbf{z})$ are the densities of the samples \mathbf{x} and \mathbf{z} of the target distribution X and the base distribution Z , respectively, and $\mathbf{J}_{\mathbf{f}^{-1}}(\mathbf{x})$ is the Jacobian of the inverse transformation \mathbf{f}^{-1} . To fit complex distributions, the diffeomorphic transformation \mathbf{f} needs to be flexible and expressive. However, expressive and yet easily invertible functions with tractable Jacobian determinants are often difficult to engineer. Fortunately, diffeomorphisms are composable, and therefore normalizing flow models can be built using compositions of simple transformations, i.e.,

$$\mathbf{f} = \mathbf{f}_K \circ \mathbf{f}_{K-1} \circ \cdots \circ \mathbf{f}_2 \circ \mathbf{f}_1, \quad (2)$$

where \mathbf{f}_1 to \mathbf{f}_K are simple diffeomorphisms and the operator \circ denotes function composition. In logarithm-

mic form, the CVF of compositions is given by

$$\log p_X(\mathbf{x}) = \log p_Z(\mathbf{f}^{-1}(\mathbf{x})) + \sum_{k=1}^K \log \left| \det \left(\mathbf{J}_{\mathbf{f}_k^{-1}}(\mathbf{x}_k) \right) \right|, \quad (3)$$

where \mathbf{x}_k is an intermediate variable $\mathbf{x}_k = \mathbf{f}_k(\mathbf{x}_{k-1})$. In practice, the transformation is often set up as a trainable function \mathbf{f}_θ with parameters θ . By using the CVF, the transformation \mathbf{f}_θ can be trained via direct likelihood maximization and for numerical reasons, the log form in Equation (3) is maximized in training:

$$\max_{\theta} \log p_X(\mathbf{x}; \theta) = \log p_Z(\mathbf{f}_\theta^{-1}(\mathbf{x})) + \log \left| \det \left(\mathbf{J}_{\mathbf{f}_\theta^{-1}}(\mathbf{x}) \right) \right| \quad (4)$$

Here, the likelihood $p_X(\mathbf{x}; \theta)$ is parameterized by the trainable parameters θ of the transformation \mathbf{f}_θ and the historical samples of the target distribution \mathbf{x} take the role of training data.

In the last six years, many flow construction methods have been proposed, e.g., [Dinh et al. \(2015\)](#) and [Dinh et al. \(2017\)](#). A prominent normalizing flow model is realNVP ([Dinh et al., 2017](#)) which uses an affine coupling layer and has shown promising results in a prior application to time series data ([Zhang and Zhang, 2020](#)). The idea of the realNVP affine coupling layer is to split the full input vector $\mathbf{z} = \mathbf{z}_{1:D}$ of dimension D and apply an affine transformation to one part of the input vector $\mathbf{z}_{d+1:D}$ conditioned on the remaining part of the input vector $\mathbf{z}_{1:d}$ that is kept constant. Here, d is usually set to $d = D/2$ to allow for maximal interaction between dimensions but can take other values $1 < d < D$, e.g., if D is uneven. The standard forward transformation $\mathbf{f}_{CL} : \mathbf{z} \rightarrow \mathbf{x}$ is given by

$$\mathbf{x}_{1:d} = \mathbf{z}_{1:d}, \quad (5)$$

$$\mathbf{x}_{d+1:D} = \exp(\mathbf{s}_\theta(\mathbf{z}_{1:d})) \odot \mathbf{z}_{d+1:D} + \mathbf{t}_\theta(\mathbf{z}_{1:d}), \quad (6)$$

where the functions $\mathbf{s}_\theta(\mathbf{z}_{1:d})$ and $\mathbf{t}_\theta(\mathbf{z}_{1:d})$ are feed-forward ANNs called conditioner networks with parameters θ and input and output dimensions d and $D - d$, respectively. The \odot operator denotes element-wise multiplication. Note that when applied as a composition in alternating form realNVP can build flexible and easily invertible transformations with tractable Jacobian determinants. A visual description of a composition of two affine coupling layers is presented in Figure 1.

The affine coupling layer in Equations (5) and (6) has the advantage that the Jacobian of the transformation \mathbf{f}_{CL} is a lower triangular matrix, i.e.,

$$\mathbf{J}_{\mathbf{f}_{CL}}(\mathbf{z}) = \begin{bmatrix} \mathbf{I} & \mathbf{0} \\ \frac{\partial \mathbf{x}_{d+1:D}}{\mathbf{z}_{1:d}} & \text{diag}[\exp(\mathbf{s}_\theta(\mathbf{z}_{1:d}))] \end{bmatrix}, \quad (7)$$

which means that the log of the absolute value of its determinant is simply given by

$$\log |\det(\mathbf{J}_{\mathbf{f}_{CL}}(\mathbf{z}))| = \sum_{i=d+1}^D \mathbf{s}_{\theta,i}(\mathbf{z}_{1:d}), \quad (8)$$

and the Jacobian of the inverse transformation $\mathbf{f}_{CL}^{-1} : \mathbf{x} \rightarrow \mathbf{z}$ satisfies

$$\log \left| \det \left(\mathbf{J}_{\mathbf{f}_{CL}^{-1}}(\mathbf{x}) \right) \right| = - \sum_{i=d+1}^D \mathbf{s}_{\theta,i}(\mathbf{x}_{1:d}), \quad (9)$$

according to the inverse function theorem ([Papamakarios et al., 2019](#)). With Equations (8) and (9), the log-Jacobian determinant is computed from a simple evaluation of the forward or inverse transformation.

For a more detailed introduction and a review of other normalizing flow designs, the interested reader is referred to the original realNVP paper by [Dinh et al. \(2017\)](#) and the review articles by [Papamakarios et al. \(2019\)](#) and [Kobyzev et al. \(2020\)](#).

3 Principal Component Density Estimation

In this section, we first extend the discussion about manifolds and normalizing flows by explaining the effects of manifolds on the Jacobians and the contradiction between manifolds and diffeomorphic transformations. Secondly, we present a novel approach for manifold density estimation by combining PCA with standard normalizing flows.

3.1 Normalizing Flows and Manifolds

Normalizing flows are transformations between the space of observable variables (target distribution) and a latent space with independent variables, i.e., a space with zero covariance (base distribution) (Papamakarios et al., 2019). As a consequence, normalizing flows disentangle the information contained in the observable variables, e.g., the power generation over a given period, to the set of independent latent variables, i.e., the normalizing flow transformation eliminates the correlation between the dimensions (Papamakarios et al., 2019; Kobyzev et al., 2020). For the disentanglement to function properly, the normalizing flow transformation \mathbf{f} and its inverse \mathbf{f}^{-1} must be continuously differentiable, i.e., the Jacobian of \mathbf{f} must be non-singular for \mathbf{f}^{-1} to be differentiable and vice versa (Papamakarios et al., 2019).

Standard normalizing flows set the latent variable space to the same dimensionality as the space of observable variables. However, for data manifolds, the actual data dimensionality embedded in the observable space is lower. Consequently, a transformation from a latent space with equal dimensionality to the space of observable variables must have a singular Jacobian, as not all of the latent variables affect the measurable variables (Hyvärinen and Pajunen, 1999). Normalizing flow transformations like realNVP (Dinh et al., 2017) are designed to be diffeomorphic between spaces of equal dimensionality. When applied to manifold data, they have to include all latent space variables in the transformation with a non-zero gradient even if the data does not show any related variance. In practice, this leads to the learned distribution being smeared out around the true distribution (Brehmer and Cranmer, 2020), causing skewed distribution densities and generation of out-of-distribution data.

3.2 Principal Component Flow Layer

Given an available injective map $\psi : \mathbb{R}^M \rightarrow \mathbb{R}^D, \mathbf{x} = \psi(\mathbf{z})$ with $D > M$ transforming data points from the lower-dimensional latent space to their full space embedding, a flow on a Riemannian manifold can be built (Gemici et al., 2016). Since the injective map expands the dimensionality, the typical CVF-relation (Equation (3)) of infinitesimal volumes using the Jacobian determinant does no longer apply. Instead, the relation between the two infinitesimal volumes is given by

$$dX = \sqrt{\det(\mathbf{J}_\psi^T \mathbf{J}_\psi)} dZ, \quad (10)$$

with Jacobian \mathbf{J}_ψ of the the mapping ψ . The generalized form of the CVF for the injective flow then is:

$$p_X(\mathbf{x}) = p_Z(\psi(\mathbf{x})^{-1}) \cdot \left[\left| \det \left(\mathbf{J}_{\psi(\mathbf{x})^{-1}}^T \mathbf{J}_{\psi(\mathbf{x})^{-1}} \right) \right| \right]^{-0.5} \quad (11)$$

As injective map, we propose the linear PCA (Pearson, 1901). The PCA is based on the singular value decomposition of the sample covariance matrix $\mathbf{K}_{X,X}$ of the data distribution X , i.e.,

$$\mathbf{K}_{X,X} = \frac{1}{N-1} \sum_{i=1}^N (\mathbf{x}_i - \boldsymbol{\mu}_X) \cdot (\mathbf{x}_i - \boldsymbol{\mu}_X)^T = \mathbf{U} \boldsymbol{\Sigma} \mathbf{V}^{-1}, \quad (12)$$

where N is the number of data points, \mathbf{x} are the data points, and $\boldsymbol{\mu}_X$ is the empirical mean vector of the distribution. The covariance matrix $\mathbf{K}_{X,X}$ is decomposed into a diagonal matrix of singular values $\boldsymbol{\Sigma}$ and two unitary matrices \mathbf{U} and \mathbf{V} of left and right singular vectors, respectively. The columns of the matrix of right singular vectors \mathbf{V} corresponding to the largest singular values are called the principal components of the data distribution X . By truncating the columns with small or zero singular values, we can use the

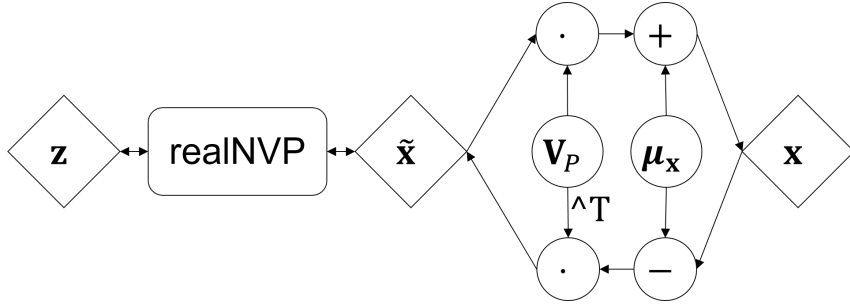


Fig. 2. Principal component flow (PCF) structure with PCA layer as last layer in generative direction and realNVP (see Figure 1) as trainable normalizing flow in lower dimensional space.

resulting semi-orthogonal matrix \mathbf{V}_P for the transformation of data points \mathbf{x} into a lower-dimensional latent space $\tilde{\mathbf{x}}$, i.e.,

$$\tilde{\mathbf{x}} = \mathbf{V}_P^T (\mathbf{x} - \boldsymbol{\mu}_X), \quad (13)$$

with \mathbf{V}_P as the truncated matrix of right singular vectors and $\boldsymbol{\mu}_X$ as the mean value of the distribution (Pearson, 1901).

Because the PCA is a linear transformation, the Jacobian $\mathbf{J}_{PCA} = \mathbf{V}_P^T$ is the transposed truncated right singular vector matrix and therefore a constant, semi-orthogonal matrix. With the Jacobian being semi-orthogonal, the determinant of the matrix $\mathbf{J}_{PCA}^T \mathbf{J}_{PCA}$ is always one, i.e.,

$$[|\det(\mathbf{J}_{PCA}^T \mathbf{J}_{PCA})|]^{-0.5} = \left[\left| \det \left(\underbrace{\mathbf{V}_P \mathbf{V}_P^T}_{=I} \right) \right| \right]^{-0.5} = 1, \quad (14)$$

independent of the considered data. When we build a composition of a standard normalizing flow and the PCA following Equation (3) it becomes apparent that the PCA transformation does not influence the CVF:

$$\begin{aligned} \log p_X(\mathbf{x}) &= \log p_Z(\mathbf{f}^{-1} \circ \mathbf{f}_{PCA}^{-1}(\mathbf{x})) + \log |\det(\mathbf{J}_{\mathbf{f}^{-1}}(\mathbf{f}_{PCA}^{-1}(\mathbf{x})))| + \underbrace{\log [|\det(\mathbf{V}_P \mathbf{V}_P^T)|]^{-0.5}}_{=0} \\ &= \log p_Z(\mathbf{f}^{-1}(\tilde{\mathbf{x}})) + \log |\det(\mathbf{J}_{\mathbf{f}^{-1}}(\tilde{\mathbf{x}}))| \end{aligned} \quad (15)$$

In Equation (15), $\tilde{\mathbf{x}} = \mathbf{f}_{PCA}^{-1}(\mathbf{x})$ is the lower dimensional representation (Equation (13)) and \mathbf{f} is a standard normalizing flow model, e.g., realNVP (Dinh et al., 2017). Note that in the composition of transformations, the PCF layer is implemented as the last layer in the generative direction. A graphical description of the combination of the PCA and realNVP is shown in Figure 2. The PCA is solved prior to fitting the normalizing flow, and the PCF layer does not include trainable variables for the log-likelihood maximization.

4 Numerical Experiments

In this section, we train the PCF on real-world time series data. The three different data sets contain data of PV power generation, wind power generation, and load demand, where each represents the total values in Germany in the years 2013 to 2015 (Open power systems data, 2019). Prior to any processing, we clean the data of any days with missing values. To our knowledge, there are no curtailment effects in the data. PV and wind scenarios are scaled by the installed capacity at each time step. Thus, the networks are trained on the so-called capacity factor. The load demand data is scaled to the $[0, 1]$ interval resulting in what we refer to as the demand factor in the following. Learning the capacity factor distribution avoids skewness of the distribution due to the addition of further generation capacity in the given time

Tab. 1. Number of principal components for cumulative explained variance (CEV). Data with 15 min resolution (96 dimensions) from [Open power systems data \(2019\)](#).

Explained variance	PV	wind	load demand
$\geq 99.00\%$	3	6	4
$\geq 99.90\%$	6	10	6
$\geq 99.99\%$	16	44	16
100.00%	62	96	96

frame. We have not observed long-term trends in the load demand data of the selected period. To be processed by the normalizing flow, the univariate time series are cut into intervals of one day each. With sampling intervals of 15 min, this leads to a set of 96-dimensional time series fragments that will serve as training data. This approach neglects that the data is a time series and treats it as a set of 96-dimensional vectors, which is a typical approach in the field of DGM scenario generation ([Chen et al., 2018c; Zhang and Zhang, 2020](#)).

First, we investigate the manifold dimensionality of the data sets by looking at the explained variance ratio of the principal components. The explained variance ratio is the value of the singular values of the covariance matrix scaled by their sum, i.e., the relative amount of variance in the data, which is described by the right singular vector (the principal component) corresponding to the given singular value ([Tipping and Bishop, 1999](#)). As an indicator of the manifold dimensionality, we look at the cumulative explained variance (CEV) which describes how much of the information in terms of variance is maintained when the data is compressed to the space of principal components. Table 1 lists some relevant CEV values and the corresponding latent space dimensionality for our data sets. The results show that a significantly reduced dimensionality is sufficient to maintain close to all of the variance information in the data. The 100 % threshold is reached when the latent dimensionality is equal to the numerical rank of the covariance matrix. The PV data reaches this threshold at a latent dimensionality of 62.

Next, we analyze generated data from the full space normalizing flow (FSNF) as well as the PCF and compare them to the historical data (target). We select two latent dimensionalities for PV (16 and 62) and one for wind and load demand (5 and 10), respectively. The latent dimensionalities for PV are selected based on the CEV analysis, whereas for wind and load demand, the latent dimensionalities are selected to highlight certain aspects of working with the PCF.

We find that for all networks five realNVP affine coupling layers with fully connected conditioner networks with two hidden layers of the same size as the input dimension each is sufficient and additional complexity does not improve the representation. All normalizing flow models are implemented using the Python-based machine learning libraries Tensorflow version 2.4.0 ([Abadi et al., 2015](#)) and Tensorflow-Probability version 0.12.1 ([Dillon et al., 2017](#)). We use the PCA routine from the open-source scikit-learn Python library version 0.24.0 ([Pedregosa et al., 2011](#)) for dimensionality reduction.

We estimate the probability density function (PDF) of the data using kernel density estimation (KDE) with Gaussian kernels ([Parzen, 1962](#)). Figures 3, 4, and 5 show PDF plots of both the historical data set and the generated scenarios with FSNF and PCF. For the PV data in Figure 3, the data from all three normalizing flow structures appear to match the distribution. The FSNF data exhibits a higher density than the target for capacity factors smaller than 0.05, between 0.1 and 0.35, and a lower density above a certain capacity factor of 0.35. The PCF62 data shows an overestimation between a capacity factor of 0.1 and 0.35, however, the PCF62 density is significantly closer to the density of the target distribution than the FSNF density. Finally, the PCF16 data distribution is closest to the target distribution with good fits for capacity factors smaller than 0.2 and similar deviations from the target as already observed with the FSNF and the PCF62.

The results for the wind capacity factor and the demand factor show similar results. In both cases, we observe an overestimation of the PDF for the highest densities and an underestimation of the tails by the FSNF. As for the PV scenarios, the density estimates for wind and load demand scenarios show an improved approximation of the distribution through dimensionality reduction with PCA although the covariance matrices are not rank deficient. It appears that the FSNF tends to ignore rare events during the likelihood maximization and thus overestimates the areas of high density. With a lower dimensionality,

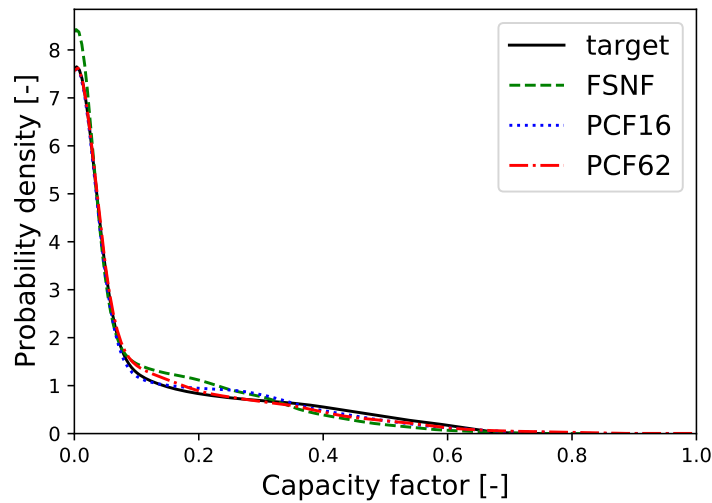


Fig. 3. PV: Probability density function of the historical data (target, bold line), generated data from full space normalizing flow (FSNF, dashed line), generated data from 16-dimensional latent space with PCF (PCF16, dotted line), and generated data from 62-dimensional latent space with PCF (PCF62, dash-dotted line).

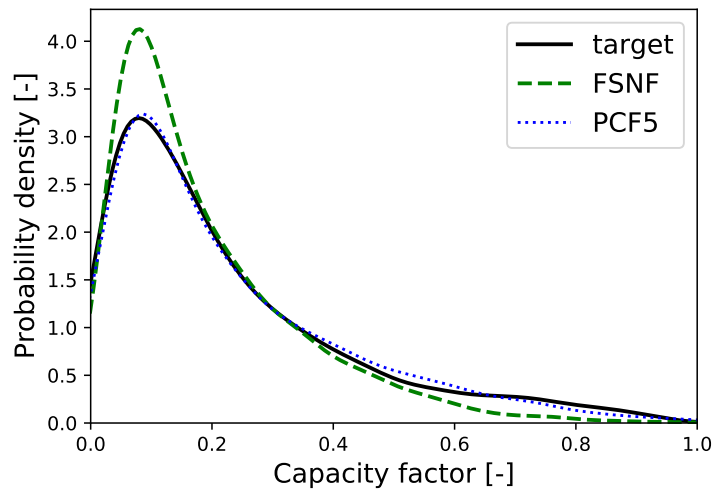


Fig. 4. Wind: Probability density function of the historical data (target, bold line), generated data from full space normalizing flow (FSNF, dashed line), and generated data from 5-dimensional latent space with PCF (PCF5, dotted line).

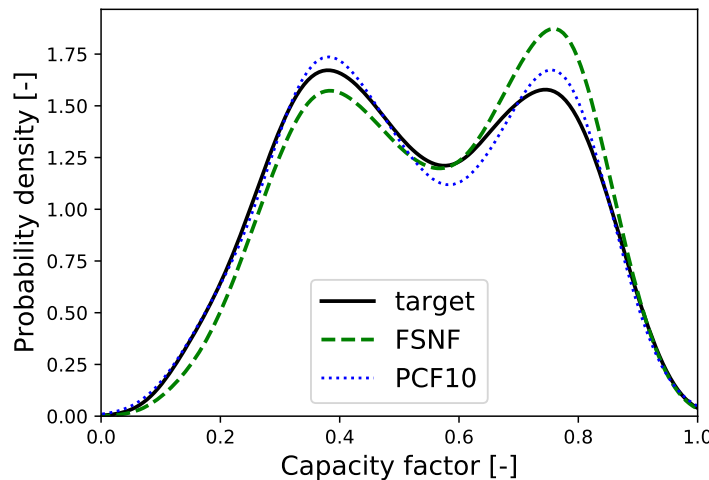


Fig. 5. Load demand: Probability density function of the historical data (target, bold line), generated data from full space normalizing flow (FSNF, dashed line), and generated data from 10-dimensional latent space with PCF (PCF10, dotted line).

rare events occupy a relatively larger space and are therefore more likely to be considered by the PCF likelihood maximization.

Note that an exact evaluation of the KDE plot can be misleading since the KDE results are not exact, in particular, at the tails of the distribution and in low-density parts (Wied and Weißbach, 2012). However, the trends for all three data sets show an improved fit of the PCF setups compared to the FSNF, which indicates better distribution fits due to the dimensionality reduction.

We use the power spectral density (PSD) based on the Welch transform (Welch, 1967) to investigate in the frequency domain whether the FSNF and the PCF can reproduce the fluctuational behavior of the original time series. Figures 6, 7, and 8 show the PSD of the target distribution, the FSNF, and the PCF generated scenarios.

For the PV data, the target distribution shows high amplitudes ($> 10^{-5}$) for low frequencies up to $\frac{1}{2.5h}$ which are well-matched by all three DGMs. For higher frequencies ($> \frac{1}{2.5h}$), the target amplitude declines faster than the FSNF amplitudes, indicating the generation of noisy behavior over shorter periods by the FSNF. In contrast, PCF16 produces lower amplitudes than the target distribution in this regime, which indicates the filtering of some of the low amplitude fluctuation in the historical data set. The PCF62 shows a good fit for the true behavior of the target up to the highest frequencies.

The PSD analysis for the wind data shows a good match of the frequency behavior for the data generated from the PCF5 and a general underestimation of the fluctuation by the FSNF. Note that the wind data exhibits higher fluctuation on all frequencies compared to the PV data. Therefore, the fluctuations at high-frequencies are represented in the principal components and no filter effect can be observed. As the overall PSD shape is matched, the FSNF appears to find the right fluctuation behavior only with consistently lower amplitudes. Here, the narrower distribution described by the FSNF (see Figure 4) leads to a smaller range of scenarios and, therefore, lower amplitudes.

The PSD analysis of the load demand data in Figure 8 highlights a potential pitfall of the PCA dimensionality reduction. While the FSNF fails to reproduce the PSD, also PCF10 exhibits fluctuations not present in the historical data surprisingly similar to the ones generated by the FSNF. Here, the linear reduction does not lead to strict filtering of noise. Instead, a reconstruction from the principal components exhibits a higher fluctuation than the original data. To illustrate this, Figure 8 also shows the PSD of the load demand data after compression to the latent space (PCA10). Since PCF10 and PCA10 exhibit the same fluctuations, the linear dimensionality reduction causes the addition of noise and not the NF. We assume the apparent similarity of the PCF10 scenarios to the FSNF scenarios to be caused by the overestimation of aspects with the highest likelihood that were already observed in the PDF.

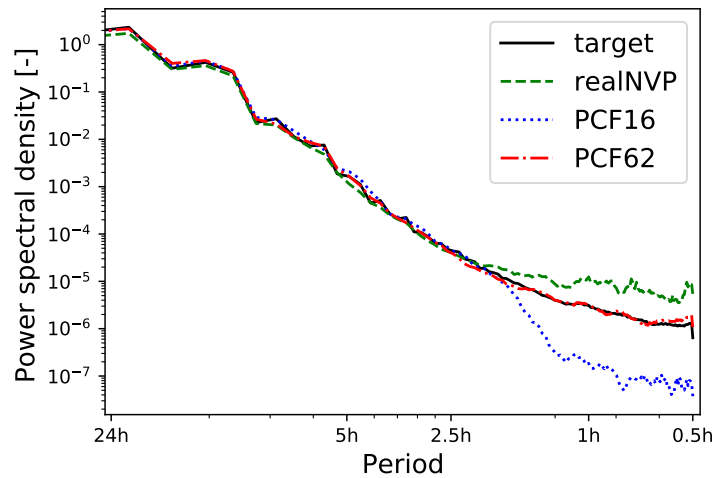


Fig. 6. PV: Power spectral density function with Welch transform (Welch, 1967) of the historical data (target, bold line) as well as of concatenated scenarios from generated data from full space normalizing flow (FSNF, dashed line), generated data from 16-dimensional latent space with PCF (PCF16, dotted line) and generated data from 62-dimensional latent space with PCF (PCF62, dash-dotted line).

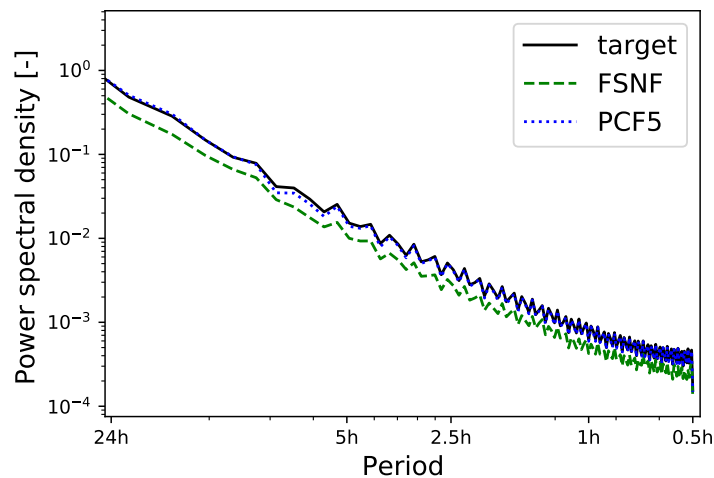


Fig. 7. Wind: Power spectral density function with Welch transform (Welch, 1967) of the historical data (target, bold line) as well as of concatenated scenarios from generated data from full space normalizing flow (FSNF, dashed line), and generated data from 5-dimensional latent space with PCF (PCF5, dotted line).

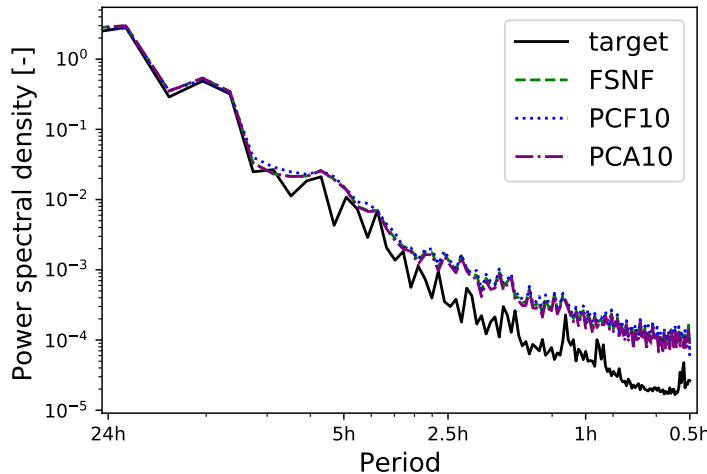


Fig. 8. Load demand: Power spectral density function with Welch transform (Welch, 1967) of the historical data (target, bold line) as well as of concatenated scenarios from generated data from full space normalizing flow (FSNF, dashed line), generated data from 10-dimensional latent space with PCF (PCF10, dotted line), and historical data after compression to a 10-dimensional latent space (PCA10, dash-dotted line).

analysis. Here, the most dominant features in the data, i.e., the behavior of the principal components, are overemphasized by the FSNF.

The PSD analysis clearly shows improved results for PV and wind data due to the dimensionality reduction, compared to the FSNF. Some effects are specific to the PCA dimensionality reduction of the given data, e.g., the filter effect observed for the PV data and the noise in the case of the load demand data. The demand data example shows that the PCF should not be applied without a prior investigation of the PCA as a suitable dimensionality reduction technique for the data at hand.

Finally, we investigate whether the PCF recovers the dimensions with zero variance which occur during the nighttime hours of the PV scenarios. Figure 9 shows the time between midnight and 4 am of five randomly selected scenarios from the historical data and the normalizing flow models. We find that the FSNF generated scenarios clearly show noisy behavior. On the other hand, PCF16 and PCF62 do not show any noise and thus preserve the zero variance feature of the respective dimensions. Figure 9 highlights the 'smeared-out' characteristic of the learned distribution as described by Brehmer and Cranmer (2020). The results show that the FSNF is unable to detect dimensions of zero variance and does not accurately fit the manifold distribution. In contrast, PCF detects the manifold and correctly reproduces its features.

5 Conclusion

In this paper, we explicate the issues associated with learning manifold data using normalizing flow density models. We find that manifold data induces ill-conditioned or singular Jacobians which interfere with the normalizing flow training. To mitigate this problem, we propose a dimensionality reducing normalizing flow layer based on the principal component analysis (PCA). The PCA does not influence the density estimation since its log-Jacobian determinant is by design always zero.

We apply the new principal component flow (PCF) next to a standard full space normalizing flow (FSNF) to learn the distribution of PV capacity factors, wind capacity factors, and load demand scenarios from Germany in the years 2013 to 2015. The results show that the PCF can generate realistic PV, wind, and load demand scenarios despite a significant dimensionality reduction, whereas the FSNF overestimates the probability density function (PDF) in areas of high density and underestimates the tails. Besides the PDF, the power spectral density (PSD) analysis reveals that PCF recovers the general periodic behavior

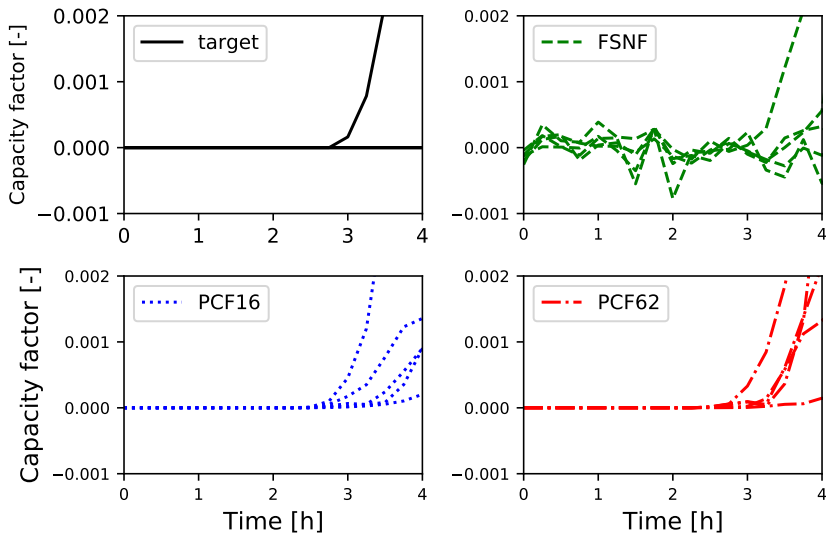


Fig. 9. Five PV scenarios from target, FSNF, PCF16 and PCF62, respectively. Time frame between midnight and 4 am.

of the time series. However, depending on the data set, the linear dimensionality reduction can introduce a potentially desired filter effect or additional noise. When applying the PCF, it is therefore important to first test how PCA-based dimensionality reduction affects the data.

Our results highlight the importance of considering the inherent latent dimensionality of the data when using normalizing flow generative models.

Acknowledgements

This work was performed as part of the Helmholtz School for Data Science in Life, Earth and Energy (HDS-LEE) and received funding from the Helmholtz Association of German Research Centres.

Nomenclature

Acronyms

ANN	Artificial neural network
CEV	Cumulative explained variance
CVF	Change of variables formula
DGM	Deep generative model
FSNF	Full space normalizing flow
GAN	Generative adversarial network
KDE	Kernel density estimation
NICE	Nonlinear independent component estimation
PV	Photovoltaic
PSD	Power spectral density
PCA	Principal component analysis
PCF	Principal component flow
PDF	Probability density function
realNVP	Real non-volume preserving transformation
VAE	Variational autoencoder

Greek letters

θ	Trainable parameters of conditioner networks s_θ and t_θ
μ_X	Mean value of distribution X
ψ	Injective transformation

Latin letters

d	Dimension
D	Dimensionality of target distribution
f	Transformation
f_{CL}	Coupling layer transformation
\mathbf{I}	Identity matrix
\mathbf{J}	Jacobian
K	Number of transformations in composition
M	Dimensionality $< D$
p_X/p_Y	Probability density of X and Y
s_θ	Conditioner network
t_θ	Conditioner network
\mathbf{V}	Matrix of right singular vectors
\mathbf{V}_P	Truncated matrix of right singular vectors
\mathbf{x}	Target distribution sample
$\tilde{\mathbf{x}}$	Compressed target distribution sample
X	Target distribution
\mathbf{z}	Base distribution sample
Z	Base distribution

Bibliography

Abadi, M., Agarwal, A., Barham, P., Brevdo, E., Chen, Z., Citro, C., Corrado, G. S., Davis, A., Dean, J., Devin, M., Ghemawat, S., Goodfellow, I., Harp, A., Irving, G., Isard, M., Jia, Y., Jozefowicz, R., Kaiser, L., Kudlur, M., Levenberg, J., Mané, D., Monga, R., Moore, S., Murray, D., Olah, C., Schuster, M., Shlens, J., Steiner, B., Sutskever, I., Talwar, K., Tucker, P., Vanhoucke, V., Vasudevan, V., Viégas, F., Vinyals, O., Warden, P., Wattenberg, M., Wicke, M., Yu, Y., and Zheng, X. (2015). TensorFlow: Large-scale machine learning on heterogeneous systems. Software available from tensorflow.org.

Agora Energiewende and Sandbag (2020). The European power sector in 2019: Up-to-date analysis on the electricity transition. *Agora Energiewende and Sandbag*, page 49.

Arjovsky, M., Chintala, S., and Bottou, L. (2017). Wasserstein GAN. *arXiv preprint arXiv:1701.07875*.

Birge, J. R. and Louveaux, F. (2011). *Introduction to stochastic programming*. Springer Science & Business Media.

Box, G. E., Jenkins, G. M., and Bacon, D. W. (1967). Models for forecasting seasonal and non-seasonal time series. Technical report, Wisconsin Univ. Madison Department of Statistics.

Brehmer, J. and Cranmer, K. (2020). Flows for simultaneous manifold learning and density estimation. *arXiv preprint arXiv:2003.13913*.

Chen, Y., Li, P., and Zhang, B. (2018a). Bayesian renewables scenario generation via deep generative networks. In *52nd Annual Conference on Information Sciences and Systems (CISS); Princeton, NJ, USA; 21-23 March 2018*, pages 1–6. IEEE.

Chen, Y., Wang, X., and Zhang, B. (2018b). An unsupervised deep learning approach for scenario forecasts. In *2018 Power Systems Computation Conference (PSCC); Dublin, Ireland; 11-15 June 2018*, pages 1–7. IEEE.

Chen, Y., Wang, Y., Kirschen, D., and Zhang, B. (2018c). Model-free renewable scenario generation using generative adversarial networks. *IEEE Transactions on Power Systems*, 33(3):3265–3275.

Chopra, I. and Selvamuthu, D. (2020). Scenario generation in stochastic programming using principal component analysis based on moment-matching approach. *OPSEARCH*, 57(1):190–201.

Dillon, J. V., Langmore, I., Tran, D., Brevdo, E., Vasudevan, S., Moore, D., Patton, B., Alemi, A., Hoffman, M., and Saurous, R. A. (2017). Tensorflow distributions. *arXiv preprint arXiv:1711.10604*.

Dinh, L., Krueger, D., and Bengio, Y. (2015). Nice: Non-linear independent components estimation. *arXiv preprint arXiv:1410.8516*.

Dinh, L., Sohl-Dickstein, J., and Bengio, S. (2017). Density estimation using real nvp. *arXiv preprint arXiv:1605.08803*.

Ge, L., Liao, W., Wang, S., Bak-Jensen, B., and Pillai, J. R. (2020). Modeling daily load profiles of distribution network for scenario generation using flow-based generative network. *IEEE Access*, 8:77587–77597.

Gemici, M. C., Rezende, D., and Mohamed, S. (2016). Normalizing flows on riemannian manifolds. *arXiv preprint arXiv:1611.02304*.

Goodfellow, I., Pouget-Abadie, J., Mirza, M., Xu, B., Warde-Farley, D., Ozair, S., Courville, A., and Bengio, Y. (2014). Generative adversarial nets. In *Advances in Neural Information Processing Systems*, pages 2672–2680.

Gu, Y., Chen, Q., Liu, K., Xie, L., and Kang, C. (2019). GAN-based model for residential load generation considering typical consumption patterns. In *2019 IEEE Power & Energy Society Innovative Smart Grid Technologies Conference (ISGT)*, pages 1–5. IEEE.

Hyvärinen, A. and Pajunen, P. (1999). Nonlinear independent component analysis: Existence and uniqueness results. *Neural networks*, 12(3):429–439.

Jiang, C., Chen, Y., Mao, Y., Chai, Y., and Yu, M. (2019). Forecasting spatio-temporal renewable scenarios: a deep generative approach. *arXiv preprint arXiv:1903.05274*.

Jiang, C., Mao, Y., Chai, Y., Yu, M., and Tao, S. (2018). Scenario generation for wind power using improved generative adversarial networks. *IEEE Access*, 6:62193–62203.

Kaut, M. and Wallace, S. W. (2003). *Evaluation of scenario-generation methods for stochastic programming*. Humboldt-Universität zu Berlin, Mathematisch-Naturwissenschaftliche Fakultät II, Institut für Mathematik.

Kaut, M. and Wallace, S. W. (2011). Shape-based scenario generation using copulas. *Computational Management Science*, 8(1-2):181–199.

Kingma, D. P. and Welling, M. (2014). Auto-encoding variational bayes. *arXiv preprint arXiv:1312.6114*.

Kobyzev, I., Prince, S. J. D., and Brubaker, M. A. (2020). Normalizing flows: An introduction and review of current methods. *arXiv preprint arXiv:1908.09257*.

Mitsos, A., Asprion, N., Floudas, C. A., Bortz, M., Baldea, M., Bonvin, D., Caspari, A., and Schäfer, P. (2018). Challenges in process optimization for new feedstocks and energy sources. *Computers & Chemical Engineering*, 113:209–221.

Open power systems data (2019). Time series. https://doi.org/10.25832/time_series/2019-06-05. Accessed: 2020-03-30.

Pan, Z., Wang, J., Liao, W., Chen, H., Yuan, D., Zhu, W., Fang, X., and Zhu, Z. (2019). Data-driven EV load profiles generation using a variational auto-encoder. *Energies*, 12(5).

Papamakarios, G., Nalisnick, E., Rezende, D. J., Mohamed, S., and Lakshminarayanan, B. (2019). Normalizing flows for probabilistic modeling and inference. *arXiv preprint arXiv:1912.02762*.

Parzen, E. (1962). On estimation of a probability density function and mode. *The Annals of Mathematical Statistics*, 33(3):1065–1076.

Pearson, K. (1901). On lines and planes of closest fit to systems of points in space. *The London, Edinburgh, and Dublin Philosophical Magazine and Journal of Science*, 2(11):559–572.

Pedregosa, F., Varoquaux, G., Gramfort, A., Michel, V., Thirion, B., Grisel, O., Blondel, M., Prettenhofer, P., Weiss, R., Dubourg, V., Vanderplas, J., Passos, A., Cournapeau, D., Brucher, M., Perrot, M., and Duchesnay, E. (2011). Scikit-learn: Machine learning in Python. *Journal of Machine Learning Research*, 12:2825–2830.

Qi, Y., Hu, W., Dong, Y., Fan, Y., Dong, L., and Xiao, M. (2020). Optimal configuration of concentrating solar power in multienergy power systems with an improved variational autoencoder. *Applied Energy*, 274:115124.

Schreiber, J., Jessulat, M., and Sick, B. (2019). Generative adversarial networks for operational scenario planning of renewable energy farms: A study on wind and photovoltaic. In *International Conference on Artificial Neural Networks*, pages 550–564. Springer.

Sharma, K. C., Jain, P., and Bhakar, R. (2013). Wind power scenario generation and reduction in stochastic programming framework. *Electric Power Components and Systems*, 41(3):271–285.

Tipping, M. E. and Bishop, C. M. (1999). Probabilistic principal component analysis. *Journal of the Royal Statistical Society: Series B (Statistical Methodology)*, 61(3):611–622.

Wang, Z., Shen, C., and Liu, F. (2018). A conditional model of wind power forecast errors and its application in scenario generation. *Applied Energy*, 212:771–785.

Wei, H., Hongxuan, Z., Yu, D., Yiting, W., Ling, D., and Ming, X. (2019). Short-term optimal operation of hydro-wind-solar hybrid system with improved generative adversarial networks. *Applied Energy*, 250:389–403.

Welch, P. (1967). The use of fast fourier transform for the estimation of power spectra: a method based on time averaging over short, modified periodograms. *IEEE Transactions on Audio and Electroacoustics*, 15(2):70–73.

Wied, D. and Weißbach, R. (2012). Consistency of the kernel density estimator: a survey. *Statistical Papers*, 53(1):1–21.

Zhang, L. and Zhang, B. (2020). Scenario forecasting of residential load profiles. *IEEE Journal on Selected Areas in Communications*, 38(1):84–95.

Zhang, Y., Ai, Q., Xiao, F., Hao, R., and Lu, T. (2020). Typical wind power scenario generation for multiple wind farms using conditional improved Wasserstein generative adversarial network. *International Journal of Electrical Power & Energy Systems*, 114:105388.

Zhang, H., Hua, W., Yub, R., Tangb, M., and Dingc, L. (2018). Optimized operation of cascade reservoirs considering complementary characteristics between wind and photovoltaic based on variational autoencoder. In *MATEC Web of Conferences*, volume 246, page 01077. EDP Sciences.